Solid State Ionics 216 (2012) 6–10

Contents lists available at SciVerse ScienceDirect

Solid State Ionics

journal homepage: www.elsevier.com/locate/ssi

Tailoring phase stability and electrical conductivity of $Sr_{0.02}La_{0.98}Nb_{1-x}Ta_xO_4$ for intermediate temperature fuel cell proton conducting electrolytes

Alma B. Santibáñez-Mendieta [a], Emiliana Fabbri [b], Silvia Licoccia [a], Enrico Traversa [a,b,*]

[a] Department of Chemical Science and Technology & NAST Center, University of Rome Tor Vergata, Via della Ricerca Scientifica 1, 00133 Rome, Italy
[b] International Center for Materials Nanoarchitectonics (MANA), National Institute for Materials Science (NIMS), 1-1 Namiki, Tsukuba, Ibaraki 305-0044, Japan

ARTICLE INFO

Article history:
Received 1 July 2011
Received in revised form 9 September 2011
Accepted 20 September 2011
Available online 21 October 2011

Keywords:
Niobate
Tantalate
Electrolyte
SOFC
Proton conductivity

ABSTRACT

$Sr_{0.02}La_{0.98}Nb_{1-x}Ta_xO_4$ (SLNT, with x = 0.1, 0.2, and 0.4) proton conducting oxides were synthesized by solid state reaction for application as electrolyte in solid oxide fuel cells operating below 600 °C. Dense pellets were obtained after sintering at 1600 °C for 5 h achieving a larger average grain size with increasing the tantalum content. Dilatometric measurements were used to obtain the SLNT expansion coefficient as a function of tantalum content (x), and it was found that the phase transition temperature increased with increasing the tantalum content, being T = 561, 634, and 802 °C for x = 0.1, 0.2, and 0.4, respectively. The electrical conductivity of SLNT was measured by electrochemical impedance spectroscopy as a function of temperature and tantalum concentration under wet (p_{H2O} of about 0.03 atm) Ar atmosphere. At each temperature, the conductivity decreased with increasing the tantalum content, at 600 °C being 2.68×10^{-4}, 3.14×10^{-5}, and 5.41×10^{-6} Scm^{-1} for the x = 0.1, 0.2, and 0.4 compositions, respectively. SLNT with x = 0.2 shows a good compromise between proton conductivity and the requirement of avoiding detrimental phase transitions for application as a thin-film electrolyte below 600 °C.

1. Introduction

The main drawbacks hindering the widespread commercialization of solid oxide fuel cells (SOFCs) are related to the high operating temperatures of conventional SOFCs that use Y-stabilized zirconia electrolytes. Lowering SOFCs operating temperature to the 400–600 °C range can reduce fabrication costs, simplify the thermal management, aid in faster start up and cool down procedures, diminish the power consumption for reaching the operating temperature, and result in less degradation of the cell and stack components [1]. Therefore, to speed up SOFC practical applications, many studies have been oriented toward the development of SOFCs working at intermediate-low temperatures (400–600 °C). For this application, high temperature proton conductors (HTPCs) are gaining growing attention as potential electrolyte materials due to the easy migration of protons inside the HTPC lattice at temperatures between 350 °C and 650 °C, which results in low activation energy for charge carrier conduction. Furthermore, the use of HTPC electrolytes allows high efficiency since water is generated at the cathode site, avoiding fuel dilution [2].

$LaNbO_4$ (LN) doped with 10 mol% Ca or 2 mol% Sr is been recently reported as a HTPC electrolyte materials stable under CO_2 and water vapor atmospheres, having a total conductivity of 2×10^{-4} Scm^{-1} in wet hydrogen at 600 °C [3, 4]. The main obstacle hindering LN practical application in SOFCs is related to its phase transition; LN shows a monoclinic (fergusonite) structure at ambient temperature and undergoes a phase transition at around 500 °C to the tetragonal (scheelite) structure [3]. The structural changes from the low temperature monoclinic phase to the high temperature tetragonal structure affect LN thermo-mechanical and conduction properties; the expansion coefficient decreases from 17.3×10^{-6} $°C^{-1}$ to 7.1×10^{-6} $°C^{-1}$ and the activation energy for proton migration changes from 0.77 eV to 0.54 eV [3]. $LaTaO_4$ (LT) is another chemically stable HTPC electrolyte, showing a total conductivity of 8×10^{-5} Scm^{-1} at 600 °C in wet hydrogen, which also shows phase transitions from orthorhombic to monoclinic at around 220 °C, and from monoclinic to tetragonal structure at about 1300 °C [5, 6]. Therefore, avoiding the phase transitions would represent a breakthrough for the development of stable electrolytes for intermediate-low temperature SOFCs.

$LaNb_{1-x}Ta_xO_4$ (LNT) single phase solid solutions can be obtained for $0\le x\le0.4$ and $0.8\le x\le0.1$, having the LN and LT crystal structure, respectively. LNT having Ta content below 40 mol% shows a linear increase in the phase transition temperature from monoclinic to tetragonal with increasing the Ta content (for x = 0, T ≈ 500 °C and for x = 0.4, T ≈ 800 °C) [5, 7], therefore it is possible to tailor the Ta content to avoid the phase transition, and thus structural changes in the desired SOFC operating temperatures.

* Corresponding author. International Center for Materials Nanoarchitectonics (MANA), National Institute for Materials Science (NIMS), 1-1 Namiki, Tsukuba, Ibaraki, 305-0044, Japan. Tel.: +81 29 860 4896; fax: +81 29 860 4706.
E-mail address: TRAVERSA.Enrico@nims.go.jp (E. Traversa).

0167-2738/$ – see front matter © 2011 Elsevier B.V. All rights reserved.
doi:10.1016/j.ssi.2011.09.019

Aim of this work is to measure the phase transition temperature and the electrical conductivity of $Sr_{0.02}La_{0.98}Nb_{1-x}Ta_xO_4$ (SLNT) solid solutions varying the tantalum content (x = 0.1, 0.2, and 0.4) to find a suitable electrolyte for operation below 600 °C.

2. Experimental

$Sr_{0.02}La_{0.98}Nb_{1-x}Ta_xO_4$ (SLNT, with x = 0.1, 0.2, and 0.4) powders were prepared by solid state reaction. Niobium (V) oxide (Nb_2O_5, 99.9%, Wako), tantalum (V) oxide (Ta_2O_5, 99.9%, Wako), lanthanum oxide (La_2O_3, 99.5%, Wako) and anhydrous strontium nitrate ($Sr(NO_3)_2$, 98%, Wako) were the starting reagents. After mixing them together in the required amounts, the mixture was subjected to ball milling for one day followed by two calcination treatments at 1400 °C for 5 h. A grinding step was performed in between the two thermal treatments. Structural characterization of the calcined powders was carried out by X-ray diffractometry (XRD, Rigaku RINT Ultima III with Cu Kα radiation).

Dense SLNT compact rectangular bars, 1 × 5 × 10 mm in size, to perform dilatometric analysis, and cylindrical pellets for conductivity measurements were obtained by pressing the powders at 230 MPa and sintering at 1600 °C for 5 h. The relative density of the SLNT sintered pellets was measured by the Archimedes method using deionized water at 22.5 °C with respect to the SLNT theoretical density of 5.897 g/cm^3 [8].

To evaluate the chemical composition and the crystalline structure of the SLNT pellets, inductively coupled plasma (ICP) analysis (optical emission spectrometer, Nippon Jarrel-Ash Co. Iris) and XRD analysis were carried out. The microstructure analysis of the SLNT sintered pellets was performed with a scanning electron microscope (SEM, Hitachi S-4800).

The transition temperature and expansion coefficient were determined with a dilatometric study, heating the sintered SLNT rectangular bars in flowing air from room temperature to 1200 °C with a heating rate of 5 °C min^{-1}, using a thermal expansion analyzer (NETZSCH, DIL402E).

For the conductivity measurements, the sintered pellets were coated on both sides with gold paste (Nilaco Corporation). The Au electrodes were firstly dried at 100 °C and then fired to 1000 °C for 10 min in air. Electrochemical impedance spectroscopy (EIS) measurements were performed using a multichannel potentiostat (Bio Logic VMP3) in wet Ar (~3% humidity) and dry Ar atmospheres over the 1 Hz–1 MHz frequency range, between 500 and 800 °C. The acquired data were fit to equivalent circuits using the Zview software [9]. Depending on the complex impedance plane plot shape, different equivalent circuits were used; at temperatures below 600 °C, the equivalent circuit (RbQb)(RgbQgb)(RpQp) was used, where Rb, Rgb, and Rp are the ohmic resistances, and Qb, Qgb, and Qp are the constant phase elements associated to the bulk, grain boundary, and electrodes, respectively. At higher temperatures, where the semiarc associated to the bulk response was not observed in the complex impedance plane plots, the Rb(RgbQgb)(RpQp) equivalent circuit was used.

3. Results and discussion

Fig. 1 shows the ambient temperature XRD patterns of $Sr_{0.02}La_{0.98-}Nb_{1-x}Ta_xO_4$ (SLNT, with x = 0.1, 0.2, and 0.4) powders. For each SLNT sample, the XRD pattern showed only the diffraction peaks corresponding to $LaNbO_4$ in monoclinic phase (space group I2/b, ICSD database no. 61013). The mean crystallite size (D) was determined using the Debye–Scherrer Eq. (1) and the Anantharaman and Christian correction Eq. (2), considering the [112] diffraction peak [10, 11].

$$D = \lambda/\beta\cos\theta \tag{1}$$

$$\beta = \left(B_{obs}{}^2 - B_{ins}{}^2\right)/B_{obs} \tag{2}$$

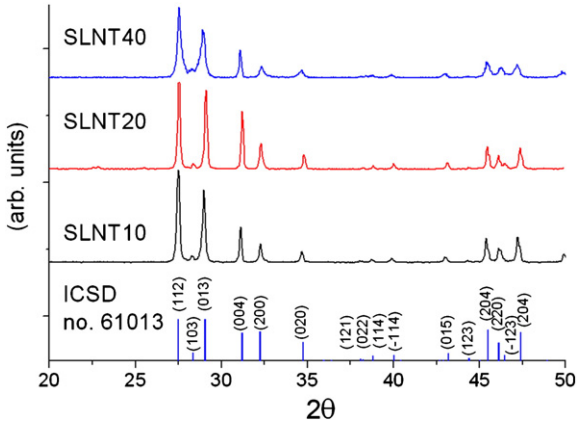

Fig. 1. XRD patterns of $Sr_{0.02}La_{0.98}Nb_{1-x}Ta_xO_4$ (SLNT, x = 0.1, 0.2, and 0.4) powders calcined at 1400 °C with a heating rate of 5 °C min^{-1}, and the ICSD pattern corresponding to the $LaNbO_4$ with monoclinic structure as a reference.

where λ is the wavelength of the X radiation (1.542 Å), θ is the peak diffraction angle (degrees), β is the corrected full width at half maximum (FWHM, radians), B_{obs} is the observed FWHM, and B_{ins} is the FWHM of the standard.

Table 1 summarizes the mean crystallite size for each SLNT composition. A decrease in the mean crystalline diameter (D) was observed with increasing the tantalum concentration up to 40 mol%.

Fig. 2 shows the XRD patterns of the SLNT pellets with different compositions. The peaks are located in the same position as in the powder patterns, indicating that single phase is retained even after the high temperature sintering, although with a smaller FWHM accounting for an increase in the crystallite size.

After grinding the pellets into powders and dissolving them with aqua regia, ICP analysis was used to verify the actual chemical composition of the SLNT sintered pellets with respect to the nominal composition. Table 2 shows that for all the SLNT samples the element concentration in the SLNT pellets was in good agreement with the nominal values.

No significant differences in the relative density values were observed among the SLNT sintered pellets, being 93% with respect to the theoretical density for the samples with x = 0.1, and 91% for both the samples with x = 0.2 and 0.4.

Fig. 3 shows the typical FE-SEM micrographs of the fractured SLNT samples sintered at 1600 °C for 5 h. For each SLNT composition, the grain size (g_i) was obtained by drawing a series of randomly distributed test lines on the images and measuring the length of the intercepted grains. The grain size distribution n(g) was determined fitting the grain size data as a log-normal distribution, as common for other sintered materials [12]. The distribution is given by Eq. (3)

$$n(g) = \frac{1}{(2\pi)^{1/2}\sigma\left(g_i/g_0\right)}\exp\left(-\frac{\left(\ln\left(g_i/g_0\right)-\mu\right)^2}{2\sigma^2}\right) \tag{3}$$

where μ and σ are the mean and standard deviation, respectively, when the natural logarithm is applied to the grain size data (g_i), and g_0 is the normalizer value equal to 1. Table 3 reports the average

Table 1
Mean crystalline diameter (D) of $Sr_{0.02}La_{0.98}Nb_{1-x}Ta_xO_4$ powders calcined in air at 1400 °C with a heating rate of 5 °C min^{-1}.

x	B (rad) × 10^3	D (nm)
0.4	3.26	48.7
0.2	1.59	99.7
0.1	2.07	76.7

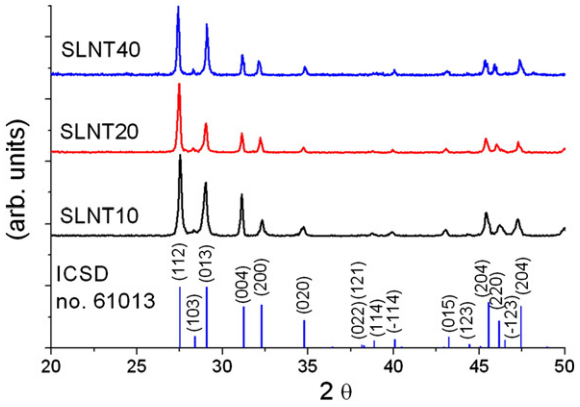

Fig. 2. XRD patterns of $Sr_{0.02}La_{0.98}Nb_{1-x}Ta_xO_4$ (SLNT, x = 0.1, 0.2, and 0.4) pellets sintered at 1600 °C for 5 h, and the reference ICSD pattern corresponding to the $LaNbO_4$ with monoclinic structure.

Table 2
ICP analysis results (mol fraction) for Sr, La, Nb and Ta contents of the $Sr_{0.02}La_{0.98}Nb_{1-x}Ta_xO_4$ (x = 0.1, 0.2, and 0.4) pellets after sintering at 1600 °C for 5 h, compared with the nominal values.

Element analyzed	SLNT10		SLNT20		SLNT40	
	Nominal	ICP	Nominal	ICP	Nominal	ICP
Sr	0.01	0.01	0.01	0.01	0.01	0.01
La	0.49	0.49	0.49	0.49	0.49	0.49
Nb	0.45	0.44	0.40	0.40	0.30	0.31
Ta	0.05	0.06	0.10	0.10	0.20	0.19

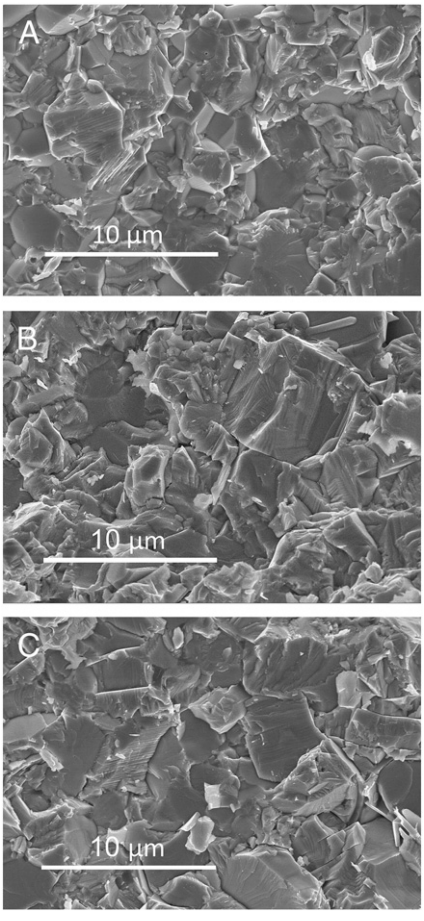

Fig. 3. SEM micrographs of the $Sr_{0.02}La_{0.98}Nb_{1-x}Ta_xO_4$ fractured pellets, with Ta content x of (A) x = 0.1, (B) x = 0.2, and (C) x = 0.4.

Table 3
Descriptive statistics obtained from the SEM images for pellets with different tantalum concentrations, calculated with different methods.

Ta	From log normal distribution fit (μm)			
(x)	g_{ave}	g_{mod}	g_{med}	sd
0.1	2.27	1.54	1.94	1.57
0.2	3.27	1.58	2.47	1.89
0.4	8.05	2.31	5.12	2.31

SLNT grain size calculated as $g_{ave} = \exp(\mu + 0.5\sigma^2)$. However this parameter is strongly influenced by the largest and smallest values, thus the mode and median values are also reported in Table 3. The mode, given as $g_{mod} = \exp(\mu - \sigma^2)$, shows the most common grain size value, while the median given by $g_{med} = \exp(\mu)$, represents the value that falls on the middle of all the measured values. Finally the standard deviation $(sd) = \exp(\sigma)$, that is a measure of the heterogeneity of the grain sizes, has been also reported in Table 3. For the SLNT samples with x = 0.1 and 0.2 all the values were similar, while larger values were found for x = 0.4, suggesting that the increase in the Ta concentration increased the grain size and grain heterogeneity.

Fig. 4 shows the cooling-stage dilatometry signal for the SLNT pellets with the typical curve slope change at the transition phase points. The same transition phase points were obtained both during heating and cooling processes. These reversible shrinkage and expansion processes are due to the SLNT phase transition, which indeed affects the oxide thermo-mechanical properties and, thus, might cause degradation of the SOFC components.

The thermal expansion coefficients of the monoclinic (α_M) and tetragonal (α_T) phases were calculated from the phase transition temperatures derived from the dilatometric curves shown in Fig. 3. Table 4 reports the phase transition temperature and the thermal expansion coefficients for each SLNT composition, which agree well with literature data for $LaNb_{1-x}Ta_xO_4$ compositions [6].

Fig. 5 shows the Arrhenius plots for the $Sr_{0.02}La_{0.98}Nb_{1-x}Ta_xO_4$ with x = 0.1, 0.2, and 0.4 under wet (Fig. 4a) and dry (Fig. 4b) argon atmospheres. For sake of comparison, Fig. 5 also reports the literature data about $Ca_{0.01}La_{0.99}NbO_4$ conductivity in wet H_2 and dry O_2 [3]. Table 5 summarizes the activation energies (Ea) obtained for the SLNT Arrhenius plots both in wet and dry atmospheres. For all the SLNT samples, the activation energy values calculated in wet Ar were smaller than those calculated in dry Ar, which is typical of proton conducting oxides. For the x = 0.1 and 0.2 compositions, a change in the activation energy was observed both in wet and dry Ar atmospheres, due to the phase transition from the monoclinic to the tetragonal phase, similarly to what reported in the literature for $Ca_{0.01}La_{0.99}NbO_4$ [3]. Since conductivity

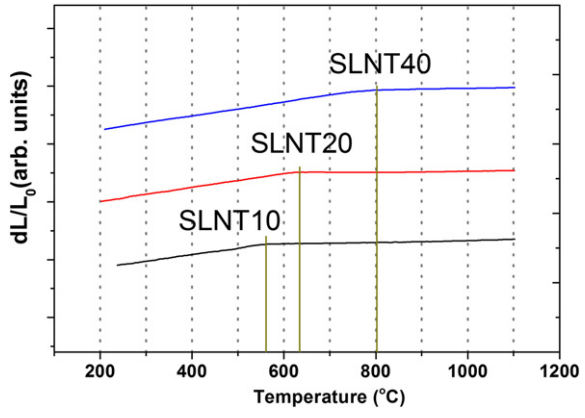

Fig. 4. Dilatometric curves during cooling from 1100 °C to 200 °C for the $Sr_{0.02}La_{0.98}Nb_{1-x}Ta_xO_4$ samples (SLNT, 10 for x = 0.1, 20 for x = 0.2, and 40 for x = 0.4).

Table 4
Phase transition temperature and expansion coefficient for the $Sr_{0.02}La_{0.98}Nb_{1-x}Ta_xO_4$ samples.

Composition (x)	Phase transition temperature (°C)	α_M $(°C^{-1})\times10^6$	α_T $(°C^{-1})\times10^7$
0.1	561	5.78	7.73
0.2	634	4.65	8.14
0.4	802	5.62	8.11

Table 5
Activation energy (Ea) of the total conductivity for different $Sr_{0.02}La_{0.98}Nb_{1-x}Ta_xO_4$ samples.

	Ar dry	Ar wet	Ar dry	Ar wet	Ar dry	Ar wet	Phase
	40%		20%		10%		
Ea (eV)			0.8890	0.7605	0.8313	0.6386	T
	1.1845	1.0773	1.1517	1.1196	1.4230	1.3442	M

measurements were performed below 800 °C, and thus below the transition temperature for SLNT40, no change in the activation energy was observed for this composition. Among the different SLNT samples, $Sr_{0.02}La_{0.98}Nb_{0.9}Ta_{0.1}O_4$ showed the largest conductivity values in both atmospheres, which is comparable with what reported in the literature for $Ca_{0.01}La_{0.99}NbO_4$ [3]. However, for $Sr_{0.02}La_{0.98}Nb_{0.9}Ta_{0.1}O_4$, the transition phase temperature of 561 °C is within the target SOFC operating temperature range, and thus this composition is not suitable for achieving continuity on thermo-mechanical properties along the whole operational temperature range. Transition phase temperatures above 600 °C were observed for the SLNT samples with tantalum concentration of 20 mol% or larger (x = 0.2 and 0.4). Under this restriction, the larger conductivity was measured for $Sr_{0.02}La_{0.98}Nb_{0.8}Ta_{0.2}O_4$, which represents therefore the best compromise between suitable electrical conductivity and thermo-mechanical properties.

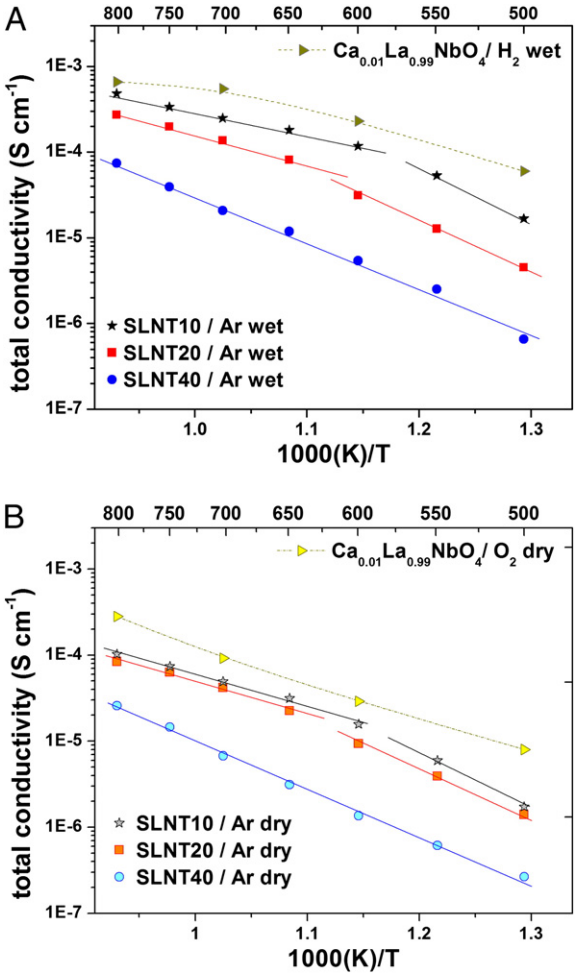

Fig. 5. Total conductivity in (A) wet argon and (B) dry argon as a function of the temperature for the $Sr_{0.02}La_{0.98}Nb_{1-x}Ta_xO_4$ (SLNT, 10 for x = 0.1, 20 for x = 0.2, and 40 for x = 0.4) pellets. The conductivity of $Ca_{0.01}La_{0.99}NbO_4$ [3] is also reported for comparison.

Figs. 6 and 7 show the impedance complex plane plots and the corresponding spectroscopic plots of the impedance imaginary part, respectively, acquired for the three SLNT pellets at 500 °C in wet Ar. Three main contributions are clearly visible for all the samples. The high frequency semiarcs, with a specific capacitance of about 10^{-12} Fcm^{-1}, can be attributed to the SLNT bulk response. The middle frequency semiarcs can be attributed to the grain boundary contribution, since the capacitance values are of about 10^{-10} Fcm^{-1}. The final spike at low frequencies can be attributed to the electrode response, as the capacitance values were calculated in the 10^{-5} Fcm^{-1} order. Table 6 summarizes the bulk and grain boundary conductivity and capacitance values for the SLNT samples.

The overall total conductivity of several ion conducting oxides is strongly affected by the grain size, and thus the grain boundary density, since grain boundaries can act as a barrier for ion transport [9, 13–16]. For SLNT pellets, the correlation between conductivity and grain size was investigated by comparing the statistical descriptors (average, mode, median and standard deviation) with the conductivity at 500 °C. The linear correlation factor between the grain boundary conductivity and the standard deviation was 0.99, suggesting that the more heterogeneous the grain size, the lower the grain boundary conductivity. Therefore, the best conductivity would be achieved by fabricating SLNT samples with a homogeneous grain size, i.e. starting from nanometric particle powders and optimizing the sintering process.

One can argue that the conductivity of the SLNT sample with 20 mol% Ta is too small for practical SOFC application at 600 °C. However, an area-specific resistance (ASR) of 0.15 Ωcm^2 is needed for an electrolyte to plan its selection for fuel cell use [17]. This value can be reached at 600 °C for the SLNT sample with 20 mol% Ta using a film having a thickness of about 50 nm. Though not trivial, this target is indeed plausible to be reached using pulsed laser deposition as the fabrication method to grow films [13], making foreseeable the practical use as a stable proton conducting electrolyte of the SLNT material in thin-film form.

4. Conclusions

$Sr_{0.02}La_{0.98}Nb_{1-x}Ta_xO_4$ materials with concentrations x = 0.1, 0.2, and 0.4 were investigated as proton conducting electrolytes with the aim to improve their thermo-mechanical stability at 600 °C,

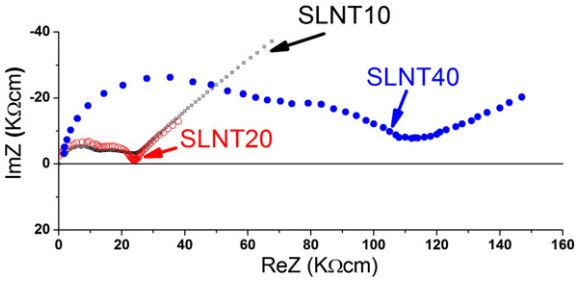

Fig. 6. Nyquist plots for the $Sr_{0.02}La_{0.98}Nb_{1-x}Ta_xO_4$ (x = 0.1, 0.2, and 0.4) pellets, measured at 500 °C in wet argon atmosphere.

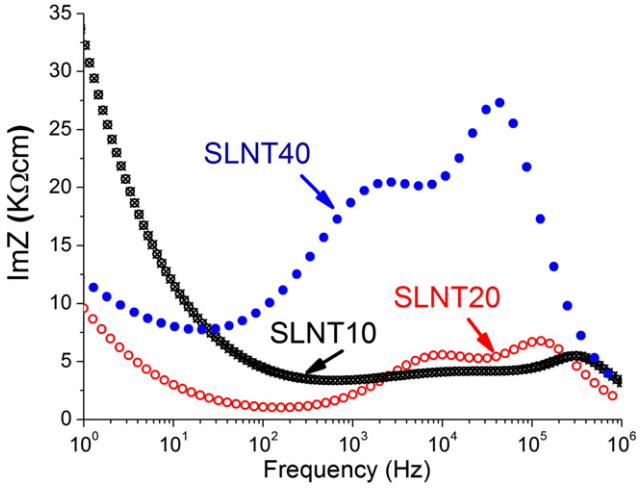

Fig. 7. Spectroscopic plots of the impedance imaginary part for $Sr_{0.02}La_{0.98}Nb_{1-x}Ta_xO_4$ (x = 0.1, 0.2, and 0.4) pellets, measured at 500 °C in wet argon atmosphere.

Table 6
Total, bulk and grain boundary conductivity and capacitance for $Sr_{0.02}La_{0.98}Nb_{1-x}Ta_xO_4$ samples, measured at 500 °C in wet argon atmosphere.

Ta (x)	Total (Scm^{-1})	Bulk		Grain boundary	
		(Fcm^{-1})	(Scm^{-1})	(Fcm^{-1})	(Scm^{-1})
0.1	1.67E-05	6.74E-12	3.17E-05	1.73E-10	2.05E-05
0.2	5.17E-06	5.41E-12	8.11E-06	3.23E-10	1.08E-05
0.4	6.58E-07	3.42E-12	1.39E-06	4.78E-10	1.24E-06

which is undermined by phase transitions. The sample with x = 0.1 composition showed the largest proton conductivity, comparable to the values reported for $Ca_{0.01}La_{0.99}NbO_4$ under H_2 wet (~2%) conditions, but the phase transition was observed at 561 °C. The SLNT sample with 20 mol% Ta composition showed suitable characteristics for practical application, with the phase transition pushed above 600 °C, the target SOFC operating temperature. However, at this temperature the total proton conductivity was measured at 3.14×10^{-5} Scm^{-1}, which allows practical applications in thin-film form of about 50 nm in thickness.

Acknowledgments

This work was supported in part by the Ministry of Foreign Affairs (MAE) of Italy under the framework of the Italy-Japan Joint Lab on Materials Nanoarchitectonics for Sustainable Development (MaNaSD), and by the World Premier International Research Center Initiative (WPI) of MEXT, Japan.

References

[1] A. Boudghene Stambouli, E. Traversa, Renewable Sustainable Energy Rev. 6 (2002) 433–455.
[2] E. Fabbri, D. Pergolesi, E. Traversa, Chem. Soc. Rev. 39 (2010) 4355–4369.
[3] R. Haugsrud, T. Norby, Nat. Mater. 5 (2006) 193–196.
[4] T. Mokkelbost, I. Kaus, R. Haugsrud, T. Norby, T. Grande, M.A. Einarsrud, J. Am. Ceram. Soc. 91 (2008) 879–886.
[5] R. Haugsrud, T. Norby, J. Am. Ceram. Soc. 90 (2007) 1116–1121.
[6] F. Vullum, F. Nitsche, S.M. Selbach, T. Grande, J. Solid State Chem. 181 (2008) 2580–2585.
[7] Z. Bi, C.A. Bridges, J.-H. Kim, A. Huq, M.P. Paranthamana, J. Power Sources 196 (2011) 7395–7403.
[8] S. Tsunekawa, H. Takei, Phys. Status Solidi A 50 (1978) 695–702.
[9] E. Fabbri, D. Pergolesi, S. Licoccia, E. Traversa, Solid State Ionics 181 (2010) 1043–1051.
[10] R. Jenkins, R. Snyder, Introduction to X-Ray Powder Diffractometry, J. Wiley and Sons, NY, 1996.
[11] E. Camargo, E. Longo, E. Leite, J. Sol-Gel Sci. Technol. 17 (2000) 111–121.
[12] R.B. Bergmann, J. Krinke, J. Cryst. Growth 177 (1997) 191–195.
[13] D. Pergolesi, E. Fabbri, A. D'Epifanio, E. Di Bartolomeo, A. Tebano, S. Sanna, S. Licoccia, G. Balestrino, E. Traversa, Nat. Mater. 9 (2010) 353–358.
[14] X. Guo, R. Waser, Prog. Mater. Sci. 51 (2006) 151–210.
[15] H.G. Bohn, T. Schober, J. Am. Ceram. Soc. 83 (2000) 768–772.
[16] H. Fjeld, D.M. Kepaptsoglou, R. Haugsrud, T. Norby, Solid State Ionics 181 (2010) 104–109.
[17] B.C.H. Steele, A. Heinzel, Nature 414 (2001) 345–352.